Magnetic control of heterogeneous ice nucleation with nanophase magnetite: Biophysical and agricultural implications

Atsuko Kobayashi[a,1], Masamoto Horikawa[b], Joseph L. Kirschvink[a,c], and Harry N. Golash[d]

[a]Earth-Life Science Institute, Tokyo Institute of Technology, Meguro, 152-8550 Tokyo, Japan; [b]Department of Systems and Control Engineering, Tokyo Institute of Technology, Meguro, 152-8552 Tokyo, Japan; [c]Division of Geological and Planetary Sciences, California Institute of Technology, Pasadena, CA 91125; and [d]Robotics Institute, Carnegie Mellon University, Pittsburgh, PA 15213

Edited by David A. Weitz, Harvard University, Cambridge, MA, and approved March 26, 2018 (received for review January 7, 2018)

In supercooled water, ice nucleation is a stochastic process that requires ∼250–300 molecules to transiently achieve structural ordering before an embryonic seed crystal can nucleate. This happens most easily on crystalline surfaces, in a process termed heterogeneous nucleation; without such surfaces, water droplets will supercool to below −30 °C before eventually freezing homogeneously. A variety of fundamental processes depends on heterogeneous ice nucleation, ranging from desert-blown dust inducing precipitation in clouds to frost resistance in plants. Recent experiments have shown that crystals of nanophase magnetite (Fe_3O_4) are powerful nucleation sites for this heterogeneous crystallization of ice, comparable to other materials like silver iodide and some cryobacterial peptides. In natural materials containing magnetite, its ferromagnetism offers the possibility that magneto-mechanical motion induced by external oscillating magnetic fields could act to disrupt the water–crystal interface, inhibiting the heterogeneous nucleation process in subfreezing water and promoting supercooling. For this to act, the magneto-mechanical rotation of the particles should be higher than the magnitude of Brownian motions. We report here that 10-Hz precessing magnetic fields, at strengths of 1 mT and above, on ∼50-nm magnetite crystals dispersed in ultrapure water, meet these criteria and do indeed produce highly significant supercooling. Using these rotating magnetic fields, we were able to elicit supercooling in two representative plant and animal tissues (celery and bovine muscle), both of which have detectable, natural levels of ferromagnetic material. Tailoring magnetic oscillations for the magnetite particle size distribution in different tissues could maximize this supercooling effect.

ice crystal nucleation | magnetic supercooling | biogenic magnetite | nanoparticles | food freezing

In water, supercooling (the retention of a liquid state at temperatures below the melting point) can be achieved only if seed nuclei can be prevented from forming. These seed crystals are commonly thought to occur either through homogeneous or heterogeneous processes. Homogeneous ice nucleation, or "spontaneous ice crystallization," is a stochastically rare event in supercooled water wherein a cluster of several hundred molecules may transiently arrange themselves into a seed crystal, leading to the sudden crystallization of the surrounding, supercooled liquid (1). Molecular and Brownian motions tend to disrupt these nascent clusters, implying that seed nuclei are more likely to form at lower temperatures where such motions are slower. Numerous studies on ultrapure water droplets show that nucleation probabilities reach stochastically high levels at about −30 to −40 °C (1, 2). In contrast, heterogeneous ice nucleation starts at the boundary between supercooled water and a solid, where the surface can help structurally organize the water molecules. This surface zone lowers the interfacial free energy during the nucleation process and rapidly increases the probability of ice formation (1, 3). Solid materials vary widely in this nucleating ability, ranging from low to nonexistent in glassy or disordered polymers, to variably high rates in crystalline solids (3–7). Factors that control this nucleation efficiency are as-yet poorly understood, but the abundant nucleation particles in ordinary tap water typically leads to ice crystal formation only slightly below the melting point at 0 °C (standard temperature and pressure).

Over the past 80 y, some of the materials shown to have high rates of heterogeneous ice nucleation include silver iodide crystals [used in cloud seeding to induce thermal convection and precipitation following the release of latent heat of crystallization (8)], proteins from cryogenically adapted bacteria [used to control freezing in some food applications (9)], as well as some minerals like feldspar (10), which may play an important climate role via cloud formation induced by Aeolian dust. More recently, Kobayashi et al. (11) demonstrated that adding nanogram/gram levels of dispersed magnetite nanocrystals (Fe_3O_4) to ultrapure water samples nearly eliminates supercooling, implying that these mineral grains also provide powerful nucleation sites for the heterogeneous crystallization of ice (11, 12), as well as reducing the volume expansion of the ice as it forms.

In natural materials containing magnetite nanoparticles, the ferromagnetic nature of this mineral offers the possibility that magneto-mechanical motion induced by external oscillating magnetic fields could act to disrupt the water molecules at the crystal/liquid interface, inhibiting the heterogeneous nucleation process and promoting supercooling. First-order dynamical estimates suggest that frequencies below <100 Hz and above

Significance

Ice crystallization affects processes as divergent as cloud formation and rain seeding, to the growth, transportation, and preservation of the human food supply. Recent estimates show that nearly 40% of all food is lost between the farm and the kitchen, and much of this is due to cellular damage from freezing. The discovery that nanocrystals of magnetite are one of nature's most potent ice nucleation materials indicates that this mineral, naturally present in many plant and animal tissues, is responsible for frost and freezer damage. As ice formed from supercooled water is less damaging to tissues, the ability to control ice nucleation with magnetic fields offers the promise of developing better technologies to minimize agricultural waste.

Author contributions: A.K. designed research; A.K. and M.H. performed research; A.K., M.H., J.L.K., and H.N.G. contributed new reagents/analytic tools; A.K. and J.L.K. analyzed data; and A.K., J.L.K., and H.N.G. wrote the paper.

The authors declare no conflict of interest.

This article is a PNAS Direct Submission.

[1]To whom correspondence should be addressed. Email: kobayashi.a.an@m.titech.ac.jp.

This article contains supporting information online at www.pnas.org/lookup/suppl/doi:10.1073/pnas.1800294115/-/DCSupplemental.

Published online May 7, 2018.

Table 1. Comparison of the rotational time constants with the average alignments given by the Langevin function: Brownian motion (τ_B)

d, nm	τ_B, ms
30	0.019
40	0.045
50	0.087
60	0.151
70	0.239
80	0.357

Calculated time constant for Brownian (thermal) motion, τ_B, for various stable, single-domain magnetite nanospheres. Note that the rate of thermal motion decreases with particle size due to increased viscous drag from the surface area.

~10 Hz might be appropriate. Here, we report experiments that confirm that ice nucleation can be delayed (e.g., supercooling can be induced) in magnetite-spiked water using 10-Hz rotating magnetic fields in the 0.5- to 1.5-mT range (e.g., 10–30 times stronger than the typical geomagnetic field of ~50 μT). Water supercooled and then frozen in this fashion displayed a similar decrease in ice volume as did the magnetite-free, supercooled control samples in previous experiments (11). These results support the hypothesis that biologically precipitated magnetite might be responsible for the effects of magnetic fields on cryopreservation and might lead to other nano-control technologies involving ice crystal nucleation. As noted explicitly by Wisniewski et al. (13), "The role of heterogeneous ice nucleators in inducing ice formation in plants is important because if methods can be developed for regulating ice nucleation, significant advances could be made in limiting frost injury to both freezing-sensitive and cold adapted plants." The identification of nanophase magnetite as a major ice nucleation agent in the natural environment, including plant and animal tissues, is a significant advance in this regard and offers the possibility of using magnetic fields to control the freezing process.

Physical Processes

Magnetite nanoparticles dispersed in water will be subjected to two major physical processes that influence their interaction with the surrounding water molecules. First, Brownian motion, particularly the particle rotations, driven by thermal agitation of the particles will tend to disrupt the surface boundary layer of water molecules and inhibit nucleation. Second, magnetite nanoparticles >30 nm in diameter lie within the single-domain stability field wherein the shape and magneto-crystalline anisotropy energies hold the net moment of the crystal fixed relative to the particle (14). The magnetic moment of the particles will interact with the ambient magnetic field, producing a torque that acts to rotate them into alignment with the field. If this field is moving, this process will contribute to the disruption of the surface layer interacting with the magnetite crystals. The balance between these time constants is given by the extension of the classical Langevin function, applied to the case of uniformly magnetized (single-domain) particles in which the magnetic anisotropy energies are large enough to pin the net magnetic moments to the crystal axes, forcing the particles to rotate; for a thorough treatment, see Coffey and Kalmykov (15).

As we anticipate that many of the crystals of biological magnetite in animal tissues would be bound to membrane systems of some sort, we note that a small force on a biological membrane will cause it to deform with a characteristic time constant of about 0.1 s (16), or a 10-Hz frequency. Hence, at higher frequencies interactions from adjacent cellular structures might damp the rotation. We also note that if these nanometer-scale particles are imbedded in stiff tissues like bone or cartilage, the supporting structures would also block their access to the diffusion of water molecules that would propagate ice nucleation. For both of these reasons, we set the frequency for our initial experiments at 10 Hz.

Magnitude of Brownian Rotation. Simulation of the Brownian motion of magnetic nanoparticles in an applied magnetic field is an important topic for numerous experiments using magnetic resonance imaging (e.g., refs. 17 and 18), and so there is an extensive literature on it. We need to know how fast these particles rotate in the surrounding water, which is the time constant for Brownian motion, τ_B. For an assemblage of freely rotating identical spheres initially held in alignment with hydrostatic volume, V ($V = 1/6\ \pi\ D^3$, where D is the diameter), in a fluid with viscosity η, the exponential time constant for the directions to randomize to the 1/e level is given by Reeves and Weaver (18) as follows:

$$\tau_B = 3\eta V/kT = \pi\eta D^3/2kT, \quad [1]$$

where k is the Boltzmann constant and T is the absolute temperature. Table 1 shows values of τ_B calculated for particles in the 30- to 80-nm size fraction that corresponds to uniformly magnetized, stable single-domain particles of magnetite. Hence, we want the magnetic time constant (needed for the magnetic torque to align particles with the applied magnetic field, considered next) to be comparable in magnitude.

Time Constant for Rotational Motion in a Magnetic Field. To produce a significant effect, the magnetic motions should be comparable or larger than those from Brownian motion. A freely rotating magnetic particle is a three-dimentional compass for which the minimum energy configuration is with the particle's magnetic moment ($\boldsymbol{\mu}$) lined up with the background magnetic field ($\mathbf{B}$). (Quantities in bold are vectors, and the rest are scalars.) When these directions are not parallel, the dipole will experience a magnetic torque that will try to bring them back into alignment. We are interested here in how fast that rotation happens, which is the time constant. Although the torque of this magnetic rotation is opposed by the viscous drag between the particle's surface and the surrounding liquid, the inertial terms are trivial in the low Reynolds number environment described by Purcell (19). Hence, the equation of motion for a magnetic sphere rotating into alignment with a local magnetic field is given by the following:

$$C\ \partial\theta/\partial t + \mu B(t)\ \sin(\theta) = 0, \quad [2]$$

where θ is the angle between the magnetic moment of the particle and the instantaneous direction of the total magnetic field, $\mathbf{B}(t)$, t is time, and C is the coefficient of rotational friction with respect to the crystal center. The instantaneous magnetic torque on the particle is then given by the vector cross-product, $\boldsymbol{\mu} \times \mathbf{B}(t)$, which is the $\mu B(t)\sin(\theta)$ term in Eq. **2**. For a spherical particle, the rotational drag coefficient, C, is given by $6\eta V$, where η is again the viscosity, and V is the volume (e.g., ref. 20), so $C = 6\eta(1/6\pi D^3) = \pi\eta D^3$. Using the standard small angle approximation where $\sin(\theta) \sim \theta$, we

Table 2. Comparison of the rotational time constants with the average alignments given by the Langevin function: Magnetic rotation (τ_m)

B, mT	τ_m, ms
0.05	4.129
0.5	0.413
1	0.206
1.5	0.138

Magnetic alignment, τ_m, in a variety of field strengths. As noted in the text, this is independent of particle size and becomes faster with increasing magnetic field strength. The two time constants are of the same order of magnitude for particles above 50 nm and in fields above 0.5 mT.

Table 3. Comparison of the rotational time constants with the average alignments given by the Langevin function: Langevin alignment (50-nm particle)

B, mT	$\xi = \mu B/kT$	$\zeta(\xi)$
0.05	0.42	0.14
0.5	4.17	0.76
1	8.33	0.88
1.5	12.50	0.92

Average alignments for ∼50-nm particles used in this study, as a function of field strength. The magnetic to thermal energy ratio, ξ, shows that the magnetic orientation exceeds the thermal disorientation for all field levels used in this study, but that the average alignment of the particles, given by the Langevin function, ζ (ξ), quickly approaches the saturation value of 1.0 in fields of ∼1 mT and above.

can get a first-order approximation of how this system behaves in a simple case, holding the magnetic field constant [e.g., assume $\mathbf{B}(t) = \mathbf{B}$]. The equation then becomes the simple first-order linear differential equation:

$$\partial\theta/\partial t + \left(\mu B/\pi\eta D^3\right)\theta = 0. \quad [3]$$

The solution to Eq. **3** is $\theta(t) = \theta_o\, e^{-t/\tau_m}$, where θ_o is the starting angular displacement, and the rotational time constant, $\tau_m = \pi\eta D^3/\mu B$. Note that τ_m does not actually depend on the particle size, as both the numerator and denominator scale with the particle volume [the magnetic moment, μ, is simply VJ_s, where J_s is the saturation magnetization of magnetite, 4.8×10^5 A/m (14)]. Using the viscosity of water at 1 °C as 1.67 mPa·s, the relationship between rotational time constant and field strength is shown in Table 2.

For magnetic fields in the 0.5- to 2-mT range, the rotational time constant is well below a millisecond. Hence, for our experiments presented below, the use of a rotating magnetic field below 100 Hz (period below 10 ms) would be slow enough for the magnetite nanoparticles to maintain a good compass alignment with the field as it changes direction.

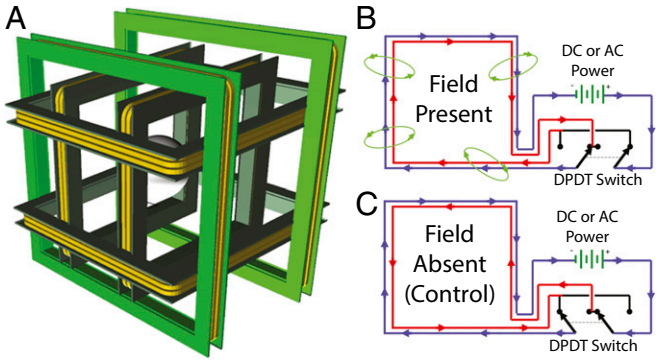

Fig. 1. Schematic diagram of the set of orthogonal square Helmholtz coils used in this study, and the wiring scheme for control experiments. (*A*) Nested square Helmholtz coils that are located within a temperature-controlled chamber inside a −80 °C freezer, as described in Fig. S1. The samples being tested for supercooling are shown by the balloon in the center of the coil system. (*B* and *C*) Coil wiring scheme using a double-pole, double-throw (DPDT) switch for controlling the active/sham states, following the recommendations for doing blinded experiments in biomagnetic studies (47). This involves the use of a double-wrapped configuration in which two strands of copper magnet wire wrapped in parallel are configured via the DPDT switch to either produce an external magnetic field (B) or a net-zero "sham" field (C), depending on the direction of current in both wires. In the sham mode, the heating and vibration artifacts are the same, but no external magnetic field is generated.

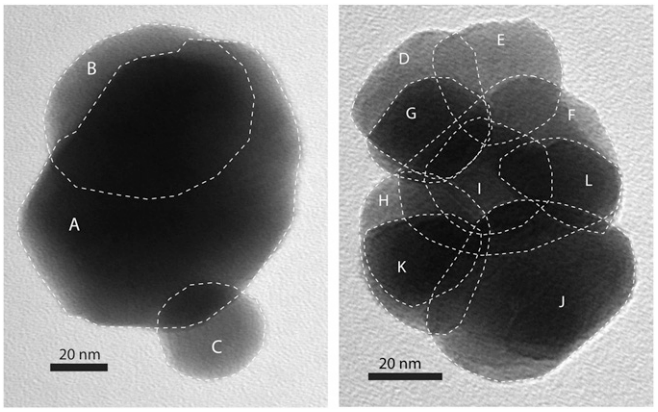

Fig. 2. TEM images of magnetite, showing the dotted outlines of the 12 crystals visible in the clumps that were used for calculating the average particle size. Note that these nanophase magnetite crystals were precipitated from dilute aqueous solution, and most likely clumped during aggregation for mounting on the TEM grids. (Scale bars: both 20 nm.)

Comparison of Time Constants and the Langevin Function. To promote supercooling, we want the magnetic field strength to be such that the induced magnetic motions will disrupt more of the incipient ice crystal nucleation sites on the surface of magnetite crystals than do the background thermal motions; for this, the timescale of magnetic rotation should be comparable to that of Brownian motion, for example, $\tau_m \sim \tau_B$. Note that the ratio $\tau_B/\tau_m = (\pi\eta D^3/2kT)/(\pi\eta D^3/\mu B) = 1/2\ (\mu B/kT)$. The ratio of magnetic to thermal energies also determines the average alignment (independent of timescale) of freely rotating magnetic moments, given by the classical Langevin theory of paramagnetism (e.g., refs. 14 and 15). If we let $\xi = uB/kT$, then the Langevin function, $\zeta(\xi) = \coth(\xi) - 1/\xi$, gives the net alignment with the applied magnetic field. As shown on Table 3, magnetic orientation dominates at field strengths above 0.5 mT for the 50-nm magnetite crystals used in the experiments described here.

Rationale for the Field and Frequency Settings Used Experimentally. To minimize the area on the surface of the magnetite crystals that remains at rest with respect to the aqueous medium, we chose to use a precessing magnetic field, composed of a static vertical component, $\mathbf{B}_v$, and a rotating horizontal component of constant magnitude, $\mathbf{B}_h$. Setting the magnitude of $\mathbf{B}_v$ equal to $\mathbf{B}_h$ yields a dip angle of the total magnetic vector with respect to horizontal of 45°. A simulation of a particle tracking this applied field is shown in Movie S1, which shows how all points on the surface of the particle have a nonzero magneto-mechanical motion added relative to the surrounding liquid. This is not the case with simple field rotation in a plane or an oscillation along one axis, as under those conditions there are spots on the particle's rotation axis that have no net motion with respect to the surrounding water, and hence might nucleate ice crystals.

From the above analysis, we chose to use ∼50-nm diameter magnetite particles, field strengths at 0.5, 1, and 1.5 mT, and 10 Hz for the rotating component of the field. Under these conditions, it is easy to show that the electrical fields induced in our balloons are far below the levels known to orient water molecules based on their slight electric dipole moments (see ref. 21 for a recent review).

A detailed description of the experimental setup as modified from Kobayashi et al. (11) is given in *SI Materials and Methods* and in Fig. S1. Fig. 1 here shows components of the magnetic exposure facility, which consists of three pairs of orthogonally nested square Helmholtz coils capable of producing static and rotating fields of up to 2 mT (20 G). Also shown is a schematic of the wiring diagram, which allows fully active and active-sham experimental modes.

ENVIRONMENTAL SCIENCES

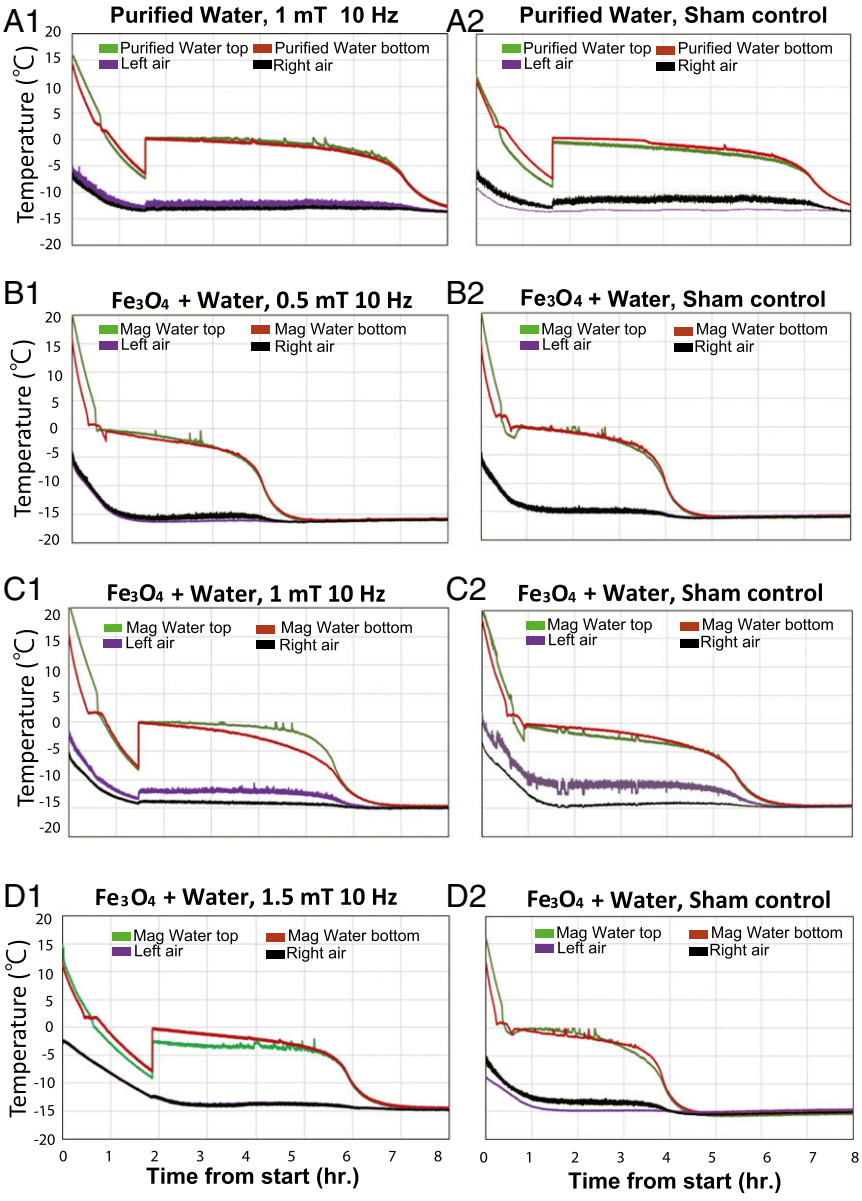

Fig. 3. Example supercooling experiments for the water samples used in this study, with summary data for all shown on Tables S1–S4. Green and red curves on all diagrams show the temperature measured at the top and bottom of the water-filled balloons vs. time; other traces are from thermocouples monitoring the background temperature in the freezing chamber. Supercooling is defined as the minimum subzero temperature reached before an ice nucleation event triggers rapid freezing. When this event occurs, the large latent heat of crystallization (~80 cal/g) makes a characteristic abrupt jump in balloon temperature up to ~0 °C. Left-hand diagrams in each pair (*A1–D1*) are from experiments in which the rotating magnetic field was at the strength and intensity indicated. Those in the right-hand column (*A2–D2*) are from the sham controls, with identical currents and frequencies to those in the paired column on the left, but with the current direction in one strand of the double-wrapped coils flowing in an antiparallel direction as indicated in Fig. 1*C*. Purified water (*A1* and *A2*) displays supercooling whether or not rotating magnetic fields are present. The addition of parts-per-billion levels of nanophase magnetite inhibits supercooling when no magnetic field is active (*B2–D2*), as noted previously (11). Addition of rotating magnetic fields above 0.5 mT (*C1* and *D1*) restores the supercooling effect, despite the presence of nanophase magnetite.

Results

Magnetite Morphology, Transmission Electron Microscopy, and Rock Magnetic Results. Fig. 2 shows transmission electron microscopy (TEM) images for two clumps of Toda magnetite particles, indicating that they are consistent with manufacturer's specifications with a nominal particle size of ~50.4 ± 20.9 nm ($n = 12$, ±1 SD). These are well within the single-domain stability field of magnetite (22). These particles presumably clumped during the aggregation process for TEM, as is well known (23), and were probably more isolated beforehand. After dilution in the ultrapure water samples following the techniques from our earlier study (11), the magnetic moment of the frozen magnetite-spiked samples measured via superconducting quantum interference device (SQUID) magnetometry was 1.5×10^{-5} Am^2/kg. As the saturation remanence for single-domain magnetite is one-half the saturation value of 92 Am^2/kg (14), this implies that the magnetite concentration was ~65 ppb (by volume), as shown on Table S5. These measurements also imply the presence of ~1 billion of the 50-nm octahedral magnetite particles per cc in the spiked water, or nearly 150 billion in each of the ~150-g balloons used in the supercooling experiments. Samples of the purified ultraclean water were comparable to instrument noise, as in our previous study (11).

Supercooling Experiments. Representative results from the water samples (pure and magnetite-spiked) are shown in Fig. 3, and numerical results for all samples are in Tables S1–S4. In Fig. 3, the left-hand side of each pair of diagrams shows results of the cooling experiments using the actively rotating magnetic fields, whereas the diagram to the right shows a corresponding control experiment with the current flowing in the "active-sham" mode. As before (11), supercooling is indicated by the drop in temperature below the 0 °C melting temperature of water, followed eventually by the freezing event and the abrupt temperature jump to 0 °C as the latent heat of crystallization (80 cal/g, or 335 J/g) is released. The first pair (Fig. 3 *A1* and *A2*) shows results from the ultrapure, magnetically clean water, which displays supercooling characteristics whether or not a rotating field is present. Fig. 3 *B–D* shows results of the magnetite-spiked water samples, with increasing field strengths of 0.5, 1.0, and 1.5 mT (5, 10, and 15 G, respectively, or 10, 15, and 20 times stronger than the typical geomagnetic field of 0.05 mT). As shown in Tables S1–S4, the ANOVA shows that the supercooling of the

magnetite-spiked water for the 0.5-mT condition was not significantly different from the sham (Tables S1–S4, bottom). However, above 0.5 mT, the supercooling is associated very strongly with the strength of the oscillating magnetic field, with the *t* test *P* values for the 1.0- and 1.5-mT comparisons with the paired sham conditions reaching values of 6×10^{-6} and 2×10^{-8}, respectively.

Cooling curves of beef and celery are shown in Figs. S2 and S3. Both displayed clear supercooling in the presence of the precessing magnetic field, but higher field strengths were needed to induce this effect in the celery.

Volumetric Change. Fig. 4 and the right-hand columns of Tables S1–S4 show results from the detailed measurement of the volume change of the balloons, before and after freezing, as a function of the lowest temperature reached before the freezing initiation event, for each of the magnetic conditions and paired shams. As in our previous study, the strongest association is with the degree of supercooling; water samples that reached lower temperature before the initiation of freezing had lower volumetric change (11). Again, the *t* test *P* values were very highly significant for the 1.0- and 1.5-mT comparisons, as shown in Tables S1–S4.

Discussion/Analysis

Our primary result that weak, rotating magnetic fields significantly inhibit ice nucleation in water spiked with nanophase magnetite confirms the hypothesis that this mineral is a powerful ice nucleation agent (11, 12). Comparison with studies of other mineral (7, 10, 24), synthetic (8), and biological agents (9) suggests that it might be among the most efficient of such materials. Additional experiments here also indicate that simple schemes involving magneto-mechanical motion of these particles in suspension, which are designed to "stir up" the water in the vicinity of the crystals beyond that already due to Brownian motion, have a strong ability to inhibit ice nucleation and promote supercooling. These experiments in particular indicate that the ice nucleation process normally happens in and around the boundary layer of water molecules that surround the magnetite mineral surface. In principle, any external action that disturbs this boundary layer ought to promote supercooling.

Our data also confirm the surprising observation that the water in these balloons expands significantly less on freezing than that in which ice nucleates at or near its melting temperature (0 °C). Conditions that promote supercooling, like purification of the water and the magnetic oscillations on magnetite-spiked water, yield this effect. As we noted previously (11), the cause of this volumetric difference is unknown but could possibly arise from trapped gasses being preferentially incorporated as clathrates (rather than forming tiny bubbles) during the rapid freezing jump. Another possibility is that the structurally disordered ice polymorph, I_{sd}, that apparently cocrystallizes with the hexagonal form (I_h) from supercooled water (25) might expand less. Whatever the mechanism, smaller changes in water volume upon freezing of plant and animal tissues from the supercooled state ought to result in less tissue damage; many studies have shown that cellular damage is minimal from tissues that were supercooled before freezing (see ref. 13 for a discussion). Coupled with a reduction in the needle-like morphology of ice I_h, our data provide a potential biophysical mechanism for past claims of magnetic fields affecting the texture of frozen plant and animal tissues, including food products (21, 26–30).

Although living organisms make nearly 60 different biominerals (31), most of them are in specialized tissues like teeth, bone, or spicules, and most are not known to promote ice crystal nucleation. For many soft tissues, the background levels of biogenic magnetite could provide the largest surface area capable of ice nucleation. Although as yet preliminary, our initial experiments on plant and animal tissues (celery and bovine muscle) show that rotating magnetic fields do indeed promote supercooling, supporting the concept that magnetite dominates the ice crystal nucleation in these materials. It is also interesting to note that our samples of celery did not supercool at the weakest field levels we used (0.5 mT) but did so at the 1.0- and 1.5-mT levels. Past studies of botanical magnetite in plants (the grasses of ref. 32) indicated that those crystals were in the 30-nm size range, rather than the ∼50-nm range used in this study. Hence, stronger fields were presumably needed to compete with Brownian motion. Detailed characterization of the natural size distribution of these magnetite particles, using well-established techniques of rock and mineral magnetism, could be used to predict the optimal magnetic conditions for damage-free cryopreservation. It would also be interesting to determine whether natural selection

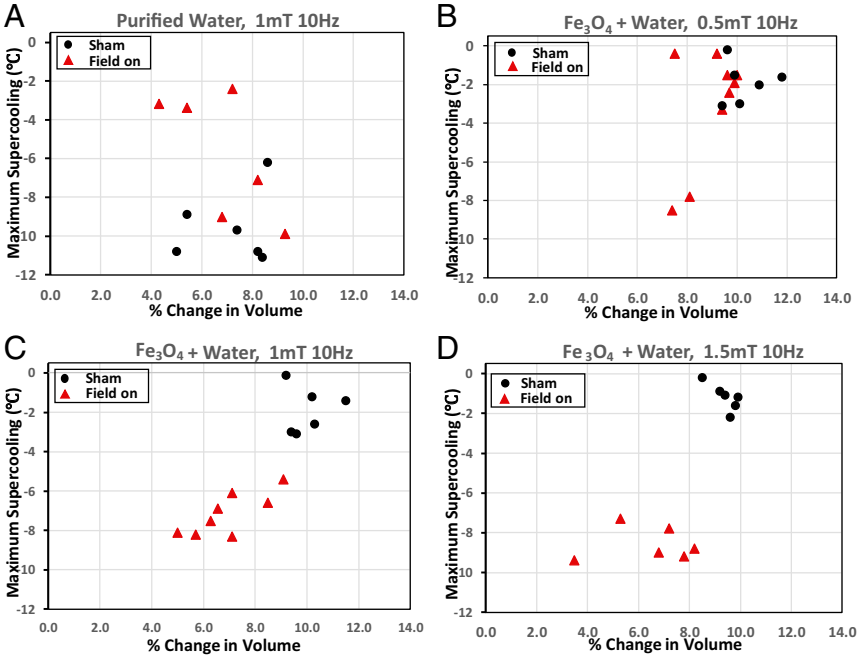

Fig. 4. Relationship between the measured volume change in the standardized polyurethane balloons and the minimum supercooling temperature reached in each experiment (data from experiments of Tables S1–S4). Note that all visible bubbles were removed from the water samples when the balloons were filled, but that any air bubbles formed during the freezing process will contribute to the measured values. (*A*) On purified water alone, rotating 1-mT, 10-Hz fields have only a slight, barely significant effect on supercooling temperature, but not volume ($P \sim 0.04$, Table S1); this is probably just chance variation. The addition of magnetite to the purified water abruptly raises both the freezing temperature and volume changes (*B*–*D*) on the sham exposures. With increasing strength of the rotating magnetic field, both the supercooling temperatures and volume changes decrease dramatically (*P* values between 10^{-2} and 10^{-7} on all four comparisons for groups *C* and *D*). The cause of these volume changes is as-yet unknown.

ENVIRONMENTAL SCIENCES

for survival in frigid environments has lowered the biological production of magnetite in the tissues of some organisms; understanding how such reduction was accomplished might aid in the development of similar traits in the human food supply. However, those implications are beyond the scope of this present work.

Gunders (33) and Gunders et al. (34) estimate that nearly 40% of farm produce in the United States is ultimately lost before it can be consumed, mostly at the production site and in the kitchen. Freezing without tissue damage can reduce these losses, so it is important to identify the physics of heterogeneous ice nucleation and identify the nucleation sites. Our data indicate that magnetite nanocrystals provide one of these important nucleation sites. Nanocrystals of magnetite form through biological processes in a variety of plant (32) and animal (35–39) tissues, including humans (40–43). This magnetite is not just for sensory purposes, as SQUID moment magnetometry reliably detects the presence of parts-per-billion to parts-per-million levels in a variety of tissues, some of which are not known to have sensory neurons [like plant tissues (32) and animal tumors (43)]. Magnetite nanoparticles of exogenous origin can also work their way into tissues (44), as appears to be the case in humans exposed to high levels of industrial pollutants (45, 46). Whatever the source, SQUID moment magnetometry on many of these typical biological tissues indicate that levels of ferromagnetic materials consistent with magnetite in the range of a few parts per billion to a few parts per million is often present in plant and animal tissues. Note that a single 50-nm crystal of magnetite in a typical ∼50-μm eukaryotic cell represents a volume fraction of only 1 ppb, but that particle could well represent the only surface capable of nucleating ice; once nucleated, the entire cell or local assembly of cells would freeze. Hence, nanocrystals of magnetite may ultimately be responsible for nucleating the ice crystals that damage biological tissues during freezing.

ACKNOWLEDGMENTS. We thank two anonymous referees for useful suggestions on the manuscript. Mr. Hiroshi Nirasawa of the Yatsugatake Chuo Agriculture Training College in Hara Village provided Nagano Japan celery samples. This study was supported by Japan Society for the Promotion of Science KAKENHI Grants JP26630062 and JP16H04276 (to A.K.).

1. Moore EB, Molinero V (2011) Structural transformation in supercooled water controls the crystallization rate of ice. *Nature* 479:506–508.
2. Atkinson JD, Murray BJ, O'Sullivan D (2016) Rate of homogenous nucleation of ice in supercooled water. *J Phys Chem A* 120:6513–6520.
3. Herbert RJ, Murray BJ, Whale TF, Dobbie SJ, Atkinson JD (2014) Representing time-dependent freezing behaviour in immersion mode ice nucleation. *Atmos Chem Phys* 14:8501–8520.
4. Earle ME, Kuhn T, Khalizov AF, Sloan JJ (2010) Volume nucleation rates for homogeneous freezing in supercooled water microdroplets: Results from a combined experimental and modelling approach. *Atmos Chem Phys* 10:7945–7961.
5. Murray BJ, Broadley SL, Wilson TW, Atkinson JD, Wills RH (2011) Heterogeneous freezing of water droplets containing kaolinite particles. *Atmos Chem Phys* 11: 4191–4207.
6. Murray BJ, et al. (2010) Kinetics of the homogeneous freezing of water. *Phys Chem Chem Phys* 12:10380–10387.
7. Harrison AD, et al. (2016) Not all feldspars are equal: A survey of ice nucleating properties across the feldspar group of minerals. *Atmos Chem Phys* 16:10927–10940.
8. Marcolli C, Nagare B, Welti A, Lohmann U (2016) Ice nucleation efficiency of AgI: Review and new insights. *Atmos Chem Phys* 16:8915–8937.
9. Cochet N, Widehem P (2000) Ice crystallization by *Pseudomonas syringae*. *Appl Microbiol Biotechnol* 54:153–161.
10. Atkinson JD, et al. (2013) The importance of feldspar for ice nucleation by mineral dust in mixed-phase clouds. *Nature* 498:355–358.
11. Kobayashi A, Golash HN, Kirschvink JL (2016) A first test of the hypothesis of biogenic magnetite-based heterogeneous ice-crystal nucleation in cryopreservation. *Cryobiology* 72:216–224.
12. Kobayashi A, Kirschvink JL (2014) A ferromagnetic model for the action of electric and magnetic fields in cryopreservation. *Cryobiology* 68:163–165.
13. Wisniewski M, et al. (2002) Extrinsic ice nucleation in plants: What are the factors involved and can they be manipulated? *Plant Cold Hardiness: Gene Regulation and Genetic Engineering*, eds Li PH, Palva ET (Kluwer Academic/Plenum Publishers, Dordrecht, The Netherlands), pp 211–221.
14. Butler RF (1992) *Paleomagnetism: Magnetic Domains to Geologic Terranes* (Blackwell Scientific Publications, Boston).
15. Coffey WT, Kalmykov YP (2012) *The Langevin Equation* (World Scientific, Singapore), 3rd Ed.
16. Hochmuth RM, Waugh RE (1987) Erythrocyte membrane elasticity and viscosity. *Annu Rev Physiol* 49:209–219.
17. Reeves DB, Weaver JB (2012) Simulations of magnetic nanoparticle Brownian motion. *J Appl Phys* 112:124311.
18. Reeves DB, Weaver JB (2015) Comparisons of characteristic timescales and approximate models for Brownian magnetic nanoparticle rotations. *J Appl Phys* 117:233905.
19. Purcell EM (1977) Life at low Reynolds number. *Am J Phys* 45:3–10.
20. Sadron C (1953) Methods of determining the form and dimensions of particls in sollution–A critical survey. *Prog Biophys Biophys Chem* 3:237–304.
21. Dalvi-Isfahan M, Hamdami N, Xanthakis E, Le-Bail A (2017) Review on the control of ice nucleation by ultrasound waves, electric and magnetic fields. *J Food Eng* 195: 222–234.
22. Butler RF, Banerjee SK (1975) Theoretical single-domain size range in magnetite and titanomagnetite. *J Geophys Res* 80:4049–4058.
23. Kobayashi A, et al. (2006) Experimental observation of magnetosome chain collapse in magnetotactic bacteria: Sedimentological, paleomagnetic, and evolutionary implications. *Earth Planet Sci Lett* 245:538–550.
24. Whale TF, et al. (2015) A technique for quantifying heterogeneous ice nucleation in microlitre supercooled water droplets. *Atmos Meas Tech* 8:2437–2447.
25. Malkin TL, et al. (2015) Stacking disorder in ice I. *Phys Chem Chem Phys* 17:60–76.
26. Abedini S, et al. (2011) Effects of cryopreservation with a newly-developed magnetic field programmed freezer on periodontal ligament cells and pulp tissues. *Cryobiology* 62:181–187.
27. Lee SY, et al. (2012) Magnetic cryopreservation for dental pulp stem cells. *Cells Tissues Organs* 196:23–33.
28. Lin PY, et al. (2013) Cryopreservation of human embryonic stem cells by a programmed freezer with an oscillating magnetic field. *Cryobiology* 66:256–260.
29. Otero L, Rodriguez AC, Perez-Mateos M, Sanz PD (2016) Effects of magnetic fields on freezing: Application to biological products. *Compr Rev Food Sci Food Saf* 15: 646–667.
30. Owada N, Saito S (2010) US Patent 7,810,340 B2.
31. Lowenstam HA, Weiner S (1989) *On Biomineralization* (Oxford Univ Press, Oxford).
32. Gajdardziska-Josifovska M, McClean RG, Schofield MA, Sommer CV, Kean WF (2001) Discovery of nanocrystalline botanical magnetite. *Eur J Mineral* 13:863–870.
33. Gunders D (2012) Wasted: How America is losing up to 40 percent of its food from farm to fork to landfill *Natural Resources Defense Council Issue Paper* (Natural Resources Defense Council, Washington, DC), IP:12-06-B.
34. Gunders D, et al. (2017) Wasted: How America is losing up to 40 percent of its food from farm to fork to landfill. Second edition of NRDC's original 2012 report. *Natural Resources Defense Council Issue Paper* (Natural Resources Defense Council, Washington, DC), IP:17-05-A.
35. Lowenstam HA (1962) Magnetite in denticle capping in recent chitons (*polyplacophora*). *Geol Soc Am Bull* 73:435–438.
36. Towe KM, Lowenstam HA (1967) Ultrastructure and development of iron mineralization in the radular teeth of *Cryptochiton stelleri* (Mollusca). *J Ultrastruct Res* 17: 1–13.
37. Presti D, Pettigrew JD (1980) Ferromagnetic coupling to muscle receptors as a basis for geomagnetic field sensitivity in animals. *Nature* 285:99–101.
38. Kirschvink JL, Jones DS, McFadden BJ (1985) *Magnetite Biomineralization and Magnetoreception in Organisms: A New Biomagnetism* (Plenum, New York).
39. Mann S, Sparks NHC, Walker MM, Kirschvink JL (1988) Ultrastructure, morphology and organization of biogenic magnetite from sockeye salmon, *Oncorhynchus nerka*: Implications for magnetoreception. *J Exp Biol* 140:35–49.
40. Kirschvink JL, Kobayashi-Kirschvink A, Woodford BJ (1992) Magnetite biomineralization in the human brain. *Proc Natl Acad Sci USA* 89:7683–7687.
41. Dobson J, Grassi P (1996) Magnetic properties of human hippocampal tissue–Evaluation of artefact and contamination sources. *Brain Res Bull* 39:255–259.
42. Dunn JR, et al. (1995) Magnetic material in the human hippocampus. *Brain Res Bull* 36:149–153.
43. Kobayashi A, Yamamoto N, Kirschvink JL (1997) Studies of inorganic crystals in biological tissue—magnetite in human tumor. *J Jpn Soc Powder Powder Metall* 44: 294–300.
44. Walker MM, Kirschvink JL, Perry AS, Dizon AE (1985) Methods and techniques for the detection, extraction, and characterization of biogenic magnetite. *Magnetite Biomineralization and Magnetoreception in Organisms: A New Biomagnetism*, Topics in Geobiology, eds Kirschvink JL, Jones DS, McFadden BJ (Plenum Press, New York), Vol 5, pp 154–166.
45. Maher BA, et al. (2016) Magnetite pollution nanoparticles in the human brain. *Proc Natl Acad Sci USA* 113:10797–10801.
46. Cohen D (1973) Ferromagnetic contamination in the lungs and other organs of the human body. *Science* 180:745–748.
47. Kirschvink JL (1992) Uniform magnetic fields and double-wrapped coil systems: Improved techniques for the design of bioelectromagnetic experiments. *Bioelectromagnetics* 13:401–411.